Research

Insights into the hierarchical geometries of hybrid low-dimensional carbons

Subhash Mandal[1,2] · Ratna Singh[2] · Debmalya Roy[2] · Kingsuk Mukhopadhyay[2] · Mayank Dwivedi[3] · Mangala Joshi[1]

Abstract

Hybrid 3D nanomaterials have been prepared by immobilizing the acid-functionalized MWCNTs into the edge-functionalized/oxidized Few Layer Graphene (FLG) flakes to address the dispersion and exfoliation of FLG flakes. Both acid-functionalized MWCNTs and the edge-oxidized FLG flakes were prepared in the laboratory. The acid-functionalized MWCNTs were prepared via oxidative treatment using a mixture of nitric acid (HNO_3) and sulphuric acid (H_2SO_4). Fenton's reaction was utilized for the preparation of the edge-oxidized FLG flakes using graphite flakes as the starting material. After the functionalization, the presence of the oxygen-containing functional groups was confirmed using FTIR spectroscopy and XPS spectroscopy. The thermal stabilities of the nanomaterials were compared using TGA thermogram and the 3D nanomaterial was observed to be more stable than any other nanoparticles that were prepared and reported in this paper. The surface morphology was observed using the SEM and TEM, and the immobilized functionalized MWCNTs between the edge functionalized FLG flakes were observed. The XRD spectra of the nanoparticles were also compared and Raman analyses have been carried out.

Keywords Carbon nanotube · Few-layer graphene flakes · Hybrid 3D nanomaterial · Spectroscopy · Microscopy

1 Introduction

The exceptional properties and unique architectures of carbon nanotubes (CNTs) have positioned them for a wide range of applications [1, 2]. However, the limited processibility of CNTs poses substantial challenges for experimental validation, especially in the realm of nanocomposites. Therefore, functionalization of CNTs emerges as a critical aspect, enhancing reactivity, facilitating uniform alignment in matrices, and fostering homogeneous dispersion in solvents [3].

A prominent method for CNT functionalization involves chemical oxidation. Datsyuk et al. [3] extensively detailed various oxidation techniques for Multi-Walled Carbon Nanotubes (MWCNTs), encompassing the utilization of piranha solution, a mixture of NH_4OH/H_2O_2, and refluxing nitric acid [3]. Notably, nitric acid exhibited enhanced defect generation on CNTs, albeit with a reduction in length. Another innovative approach employs potassium permanganate supported by a phase transfer catalyst (PTC) [4, 5]. This method, as employed by Zhang et al. resulted in a noteworthy 30% increase

---

✉ Debmalya Roy, droy.dmsrde@gov.in; ✉ Mangala Joshi, mangala@textile.iitd.ac.in | [1]Department of Textile and Fiber Engineering, Indian Institute of Technology Delhi, New Delhi, India. [2]Nano Science & Coating Division (NSCD), Defence Materials and Stores Research & Development Establishment (DMSRDE), DRDO, Kanpur, India. [3]DMSRDE, DRDO, Kanpur, India.

in functionalization yield. The optimized oxidation process, facilitated by PTC, thus presents itself as a viable and cost-effective method for the large-scale production of high-quality functionalized CNTs [4].

Consideration is also given to graphite nanoplatelets, deemed cost-effective fillers with promising properties for composites. At the nanoscale, graphite, when exfoliated, yields nanoplatelets composed of a few graphene layers [6]. The synthesis of graphene involves overcoming substantial van der Waals forces between graphite layers, requiring a considerable amount of energy for the release of individual graphene sheets [7, 8]. Ultrasonication stands out as a mild technique for graphite exfoliation [8]. In a detailed study tracking the impact of ultrasonication duration and power on the generation of defects on exfoliated graphene, insights were gained, revealing that prolonged ultrasonication or high power levels could lead to the decomposition of oxygen-containing functional groups to some extent, creating more defects on the graphene lattice [9].

Graphene, although present in nature, necessitates physical or chemical processes for the exfoliation of graphite and obtaining graphene layers [10]. A cost-effective and bulk-feasible approach involves the chemical reduction of graphene oxide (GO) to generate reduced graphene oxide (rGO) [11]. Various processes for oxidizing graphite to synthesize GO were developed by Hummers, Brodie, and Staudenmeier, with the Hummers method being the most significant and widely used [12–14]. However, it is not without drawbacks, including the generation of toxic gases and challenges in eliminating ions during the GO creation and cleaning process. An improved Hummers method, developed for GO production without using $NaNO_3$, offers a cleaner process without the emission of toxic gases and simplified waste liquid purification, making GO production more economical [15, 16].

GO itself is a non-conductor of electricity and lacks stability at high temperatures. Nevertheless, its electrical conductivity and thermal stability can be restored through chemical reduction, with hydrazine being a popular reducing agent [17–19]. However, the practical uses of hydrazine are limited due to its hazardous nature and high sheet resistance [20, 21]. Stankovich et al. identified hydrazine hydrate as a superior reducing agent for creating thin graphene-like sheets with electrical conductivity [22, 23]. rGO, produced by reducing exfoliated GO sheets in water containing hydrazine, exhibits a large specific surface area and can be used as a conductive filler for nanocomposites or for hydrogen storage.

Exploration into the reduction process of GO also includes sodium borohydride ($NaBH_4$) as a reducing agent [24]. Compared to hydrazine, $NaBH_4$ was found to result in lower sheet resistance and better conductivity in reduced GO films. Shen et al. introduced a simple, quick, and economic technique for producing GO by reacting graphite with benzoyl peroxide, fully exfoliating GO into sheets, and then reducing them in situ into rGO nanoplatelets using $NaBH_4$ [25]. This method allows control over the degree of functionalization and facilitates the production of stable GO without solvents, opening avenues for various applications when paired with other bulk production techniques.

Solution-based chemical reduction of graphene oxide (GO) offers economic and large-scale production benefits, but agglomeration occurs due to the high π-π stacking affinity of reduced graphene oxide (rGO) sheets. Capping agents are often employed to mitigate this issue. While hydrazine hydrate has been widely used as a reducing agent for GO, its noxious nature necessitates safety precautions. In response to this, L-ascorbic acid, a naturally occurring and non-hazardous reducing agent, has been explored for GO reduction [26]. Zhang et al. demonstrated a simple aqueous reduction method using L-ascorbic acid at room temperature, resulting in a notable restoration of electronic conjugation in rGO and significant removal of oxygen-containing functional groups [27–31]. Stable reduced GO sheets were obtained without capping agents, suggesting that the oxidized products of L-ascorbic acid may function as capping agents [32, 33].

The Fenton reaction [34], particularly the photo-Fenton reaction, has been utilized to transform GO into nanoporous graphene sheets under benign conditions [35, 36].

The synthesis and characterization of nano-porous carbonaceous nanofillers, such as f-FLG flakes, have been explored as well. Functionalization of CNTs using a mixture of acids (H_2SO_4 and HNO_3) results in oxidized CNTs with increased carboxylic acid groups. The oxidation process involves defect generation and consumption, targeting the graphene structure and forming active sites. Sonication in H_2SO_4/HNO_3 leads to defect generation at existing and newly developed sites along the CNT walls. The sonochemical approach is employed for the generation of defects on the graphitic lattice, as well as the creation of carbon–metal nanoparticle interfaces for FLG synthesis with edge functionalization. The graphite lattice is delaminated and functionalized through the graphite-iron nanoparticles interface. This physicochemical process targets nano-sized carbon–metal nanoparticle interfaces for the generation of FLG with functionalization mainly at the edges [37, 38].

Various studies have explored the acid functionalization of CNTs [39], investigated their morphological characteristics [40], developed high-performance nanocomposite membranes using hydroxylated graphene and graphene oxide [41], demonstrated the biocompatibility of hydroxylated graphene [42], and fabricated flexible carbon films with ultrahigh electrical and thermal conductivity based on hydroxylated graphene [43].

In our previous studies, we have synthesized, modified, and functionalized nanomaterials, including acid-functionalized MWCNTs as well as edge-functionalized/oxidized graphene flakes [44, 45]. The challenge of graphene exfoliation is a significant issue. The main objective of this work is to address the dispersion and exfoliation challenges of FLG flakes. For this hybrid, 3D nanomaterials have been prepared by immobilizing acid-functionalized MWCNTs into hydroxylated FLG flakes; subsequently, their microstructural properties have been evaluated and reported. The acid-functionalized MWC-NTs and hydroxylated FLG flakes have been considered to establish hydrogen bonding between carboxy and hydroxyl group after immobilization of acid-functionalized MWCNTs into hydroxylated FLG flakes for chemically stable structure. The immobilizing of acid-functionalized MWCNTs into hydroxylated FLG flakes also makes the hybrid 3D nanomaterial porous and exfoliation of the graphene of the FLG flakes.

2 Experimental work

2.1 Materials used

Synthetic graphite powder with a flake size of approximately 20 μm was obtained from Sigma-Aldrich, India, with a purity level of 99.99%. Additionally, the laboratory synthesized, modified, and functionalized nanomaterials, including acid-functionalized MWCNTs with an outer diameter of 30–40 nm and a length of 3–4 μm, as well as edge-functionalized/oxidized graphene flakes with a size ranging from 500 to 1000 nm and approximately 10–15 graphene layers [44, 45] were used for this work.

2.2 Preparation of functionalized MWCNTs by oxidative treatment [46]

In a glass flask of 25 mL, 10 mg of MWCNTs was weighed and added. Along with MWCNTs, 0.6 mL of DI water, 9.4 mL of HNO_3 (69%) and 8.0 mL of H_2SO_4 (96.2%) were added to the glass flask. Thus, an acidic solution of 18 mL volume was created which consisted of 8.0 M HNO_3 and 8.0 M H_2SO_4. The MWCNTs containing solution was initially stirred for 1 min. Then the solution was sonicated (40 kHz, 130 W) for 5 min so as to disperse the MWCNTs. In order to disperse the agglomerated MWCNTs, the cycle consisting of mixing and dispersion was carried out two times. The solution was then sonicated and the bath temperature was increased and maintained at 60 °C during the course of the treatment. This process was carried out for 2 h. Once the surface was treated, the MWCNTs were removed from the acidic solution by centrifuging at 4500 rpm, and washed with DI water several times and dried. The final product was looking like black powder. Figure 1 shows the schematic of functionalization of MWCNTs.

2.3 Preparation of edge functionalized/oxidized Few Layer Graphene (FLG) flakes

We employed ultra-sonication to sonochemically generate nanoparticles of iron oxide and iron on the flakes of graphite. A solution is prepared by dissolving $Fe(SO_4)0.7H_2O$ (8.9 gm) and a small amount (1–2 mL) of ethanol in DI water (20 L) and graphite powder (8 gm) was added to it. The solution was then ultrasonicated at 20 kHz for one hour in inert atmosphere. Next, 180 mL of 30% H_2O_2 was divided into nine equal portions and each portion was added every hour to the ultra-sonicated solution with rigorous stirring. We added 30% sulphuric acid (18–20 mL) and kept the pH of the reaction mixture at 3–4 in order to dissolve the iron salts. The Fenton's reaction solution was continuously stirred for 48 h. After allowing the reaction solution to settle for 15 min, it was decanted and filtered to obtain edge-functionalized FLG flakes. After multiple washes with DI water and warm water/alcohol, the sample was dried at 60 °C overnight. It was further rinsed with warm HCl/H_2O_2 after which it was repetitively centrifuged. Subsequently, the sample was dried and then sonicated for 30 min in N,N-dimethyl formamide (DMF) at a concentration of 0.25 mg/ml. It was centrifuged for 15 min at 1000 rpm and the FLG flakes with edge-functionalization were recovered from the supernatant of the solution which was then vacuum-dried. The final product was looking like black powder. Representation of the process of synthesis of edge-functionalized FLG flakes is shown in Fig. 2.
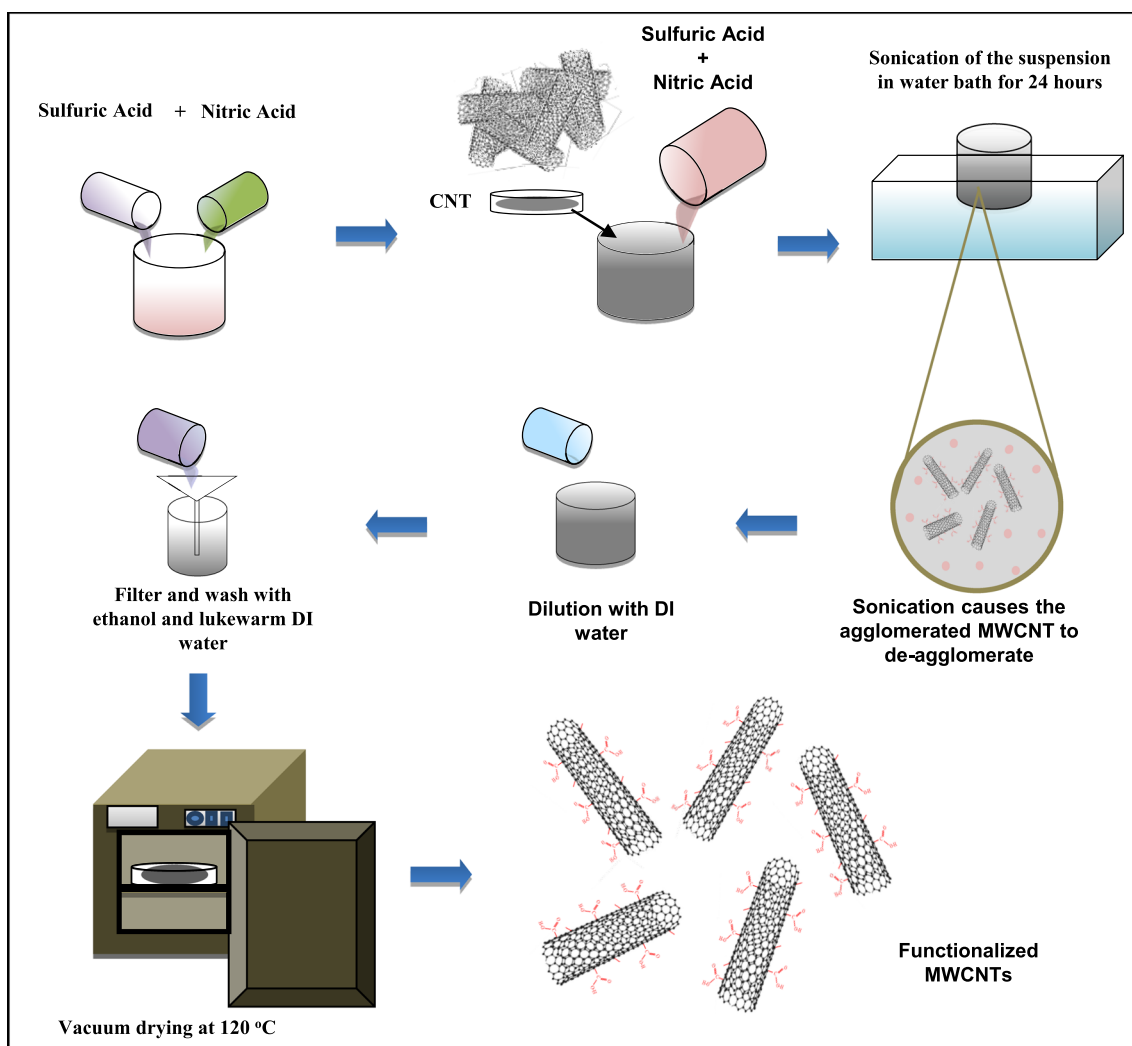
Fig. 1 Schematic of chemical oxidation (functionalization) of MWCNTs

2.4 Preparation of hybrid 3D nanomaterials

The functionalized MWCNTs was synthesized and it was then taken in a beaker in DMF. This mixture was sonicated for 30 min in order to achieve proper dispersion. The edge-functionalized/oxidized FLG flakes were synthesized and added to the functionalized MWCNTs in DMF solution. The functionalized MWCNTs and the edge-functionalized FLG were added in 25/75, 50/50 and 75/25 weight ratio. The solution was again sonicated for 30 min. The solution was vacuum dried overnight at 70 °C, and the 3D nanomaterial was obtained and stored in air-tight containers. The final product was looking like black powder. Figure 3 shows the graphical representation of the synthesis procedure of 3D hybrid nanomaterials.

2.5 Characterization of nanomaterials

ATR-FTIR spectra were acquired using a high-resolution ATR-FTIR instrument (Spectrum 100 series, Perkin Elmer) with a scanning range of 4000–600 cm^{-1}, a resolution of 4 cm^{-1}, and an average of 8 scans per sample. The ATR element employed was a zinc selenide (ZnSe) crystal. Morphological studies and analysis were conducted through scanning electron microscopy (SEM) on a Carl Zeiss scanning electron microscope (SUPRA 40 VP, Gemini) at an acceleration voltage of 25 kV. Prior to SEM studies, all test samples underwent vacuum gold sputtering. X-ray diffraction (XRD)
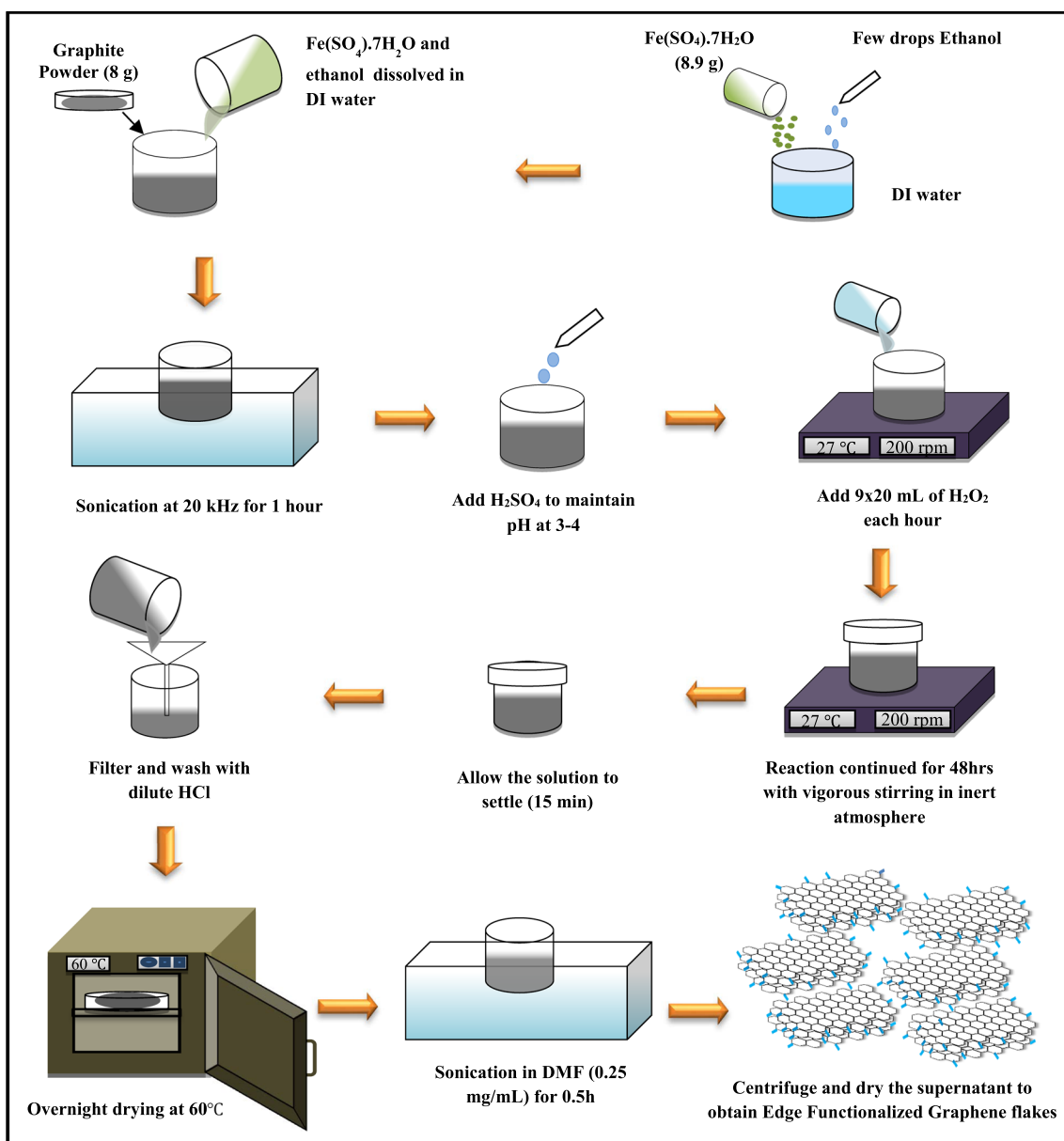
Fig. 2 Process of synthesis of edge-functionalized FLG flakes

patterns of carbonaceous nanomaterials were obtained using a Bruker AXS diffractometer (D8 Advanced) in Germany. The X-ray source had a wavelength of 0.154 nm (Cu K-alpha) generated in a sealed tube. Transmission electron microscopy (TEM) samples were prepared by drop casting on a carbon-coated copper grid with a mesh size of 300 and analyzed using a TEM (JEM-2010, JEOL, Japan) operated at a 200 kV accelerating voltage. Thermogravimetric analysis (TGA) was conducted in a TA-2920 analyzer at a heating rate of 10 °C/min. Sample preparation involved using compounded materials, and TGA was performed in an xygen atmosphere with a volumetric flow rate of 60 cm^3/min. Raman spectra of powder samples were recorded using a Renishaw Raman Microscope with Ar-ion laser excitation at 514 nm and a power of 50 mW. X-ray photoelectron spectroscopy (XPS) experiments were carried out using a VSW spectrometer with AlKa radiation. The spectral resolution was 0.6 eV at 530 eV binding energy. The chamber's base pressure was maintained at ~4×10^{-10} torr, and spectra were recorded immediately upon activating the X-ray source to prevent induced artefacts. For survey and carbon core level analysis, a take-off angle of 45 degrees and pass energy of 58.7 eV were employed. To preserve the surface composition, Ar ion sputtering was avoided during sample surface cleaning.
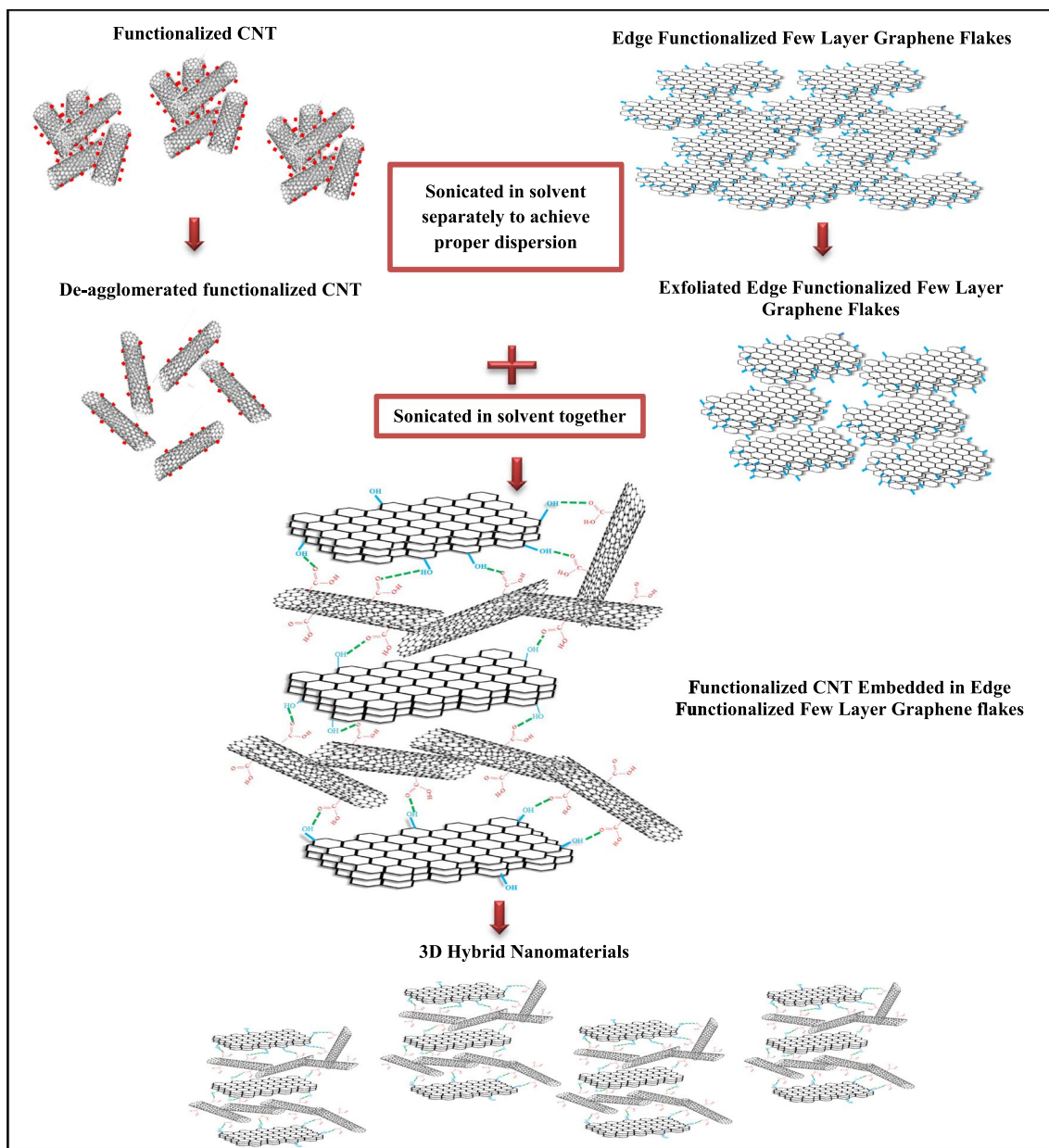
Fig. 3 Graphical representation of synthesis procedure of 3D hybrid nanomaterials

3 Results and discussion

The hybrid 3d nanofillers have been prepared in three different compositions viz. (i) 25/75, (ii) 50/50 and (iii)75/25 using acid-functionalized MWCNTs and hydroxylated FLG flakes. The composition 25/75 was found to dominate by hydroxylated FLG while 75/25 was observed to dominate by acid-functionalized MWCNTs. However, the 50/50 composition was found optimized where the acid-functionalized MWCNTs were found to penetrate and immobilize into the hydroxylated FLGs. These observations based on SEM and TEM for compositions of 25/75 and 75/25 have been provided in the supplementary information to restrict the length of the manuscript while the optimized composition i.e. 50/50 has been included and described in the manuscript. The electron microscopic images of hybrid 3D nanofillers—(a) SEM (25/75), (b) TEM (25/75), (c) SEM (75/25) and TEM (75/25) have been provided in Figure S1.

3.1 Attenuated total reflection-fourier transform infrared (ATR-FTIR)

ATR-FTIR analysis is done to determine the different kinds of bonds present in the sample. The acid treatment of MWCNTs introduces different oxygen containing functional groups like carboxyl functional group (–COOH) onto the surface of carbon. The FTIR analysis confirmed the presence of functional groups by comparing the spectra of the un-functionalized MWCNTs and the functionalized MWCNTs, as shown in Fig. 4a, b. The strong intensity peak at wavenumber ~ 3400 cm^{-1} increased due to stretching of the –OH bond of carboxyl group (–COOH). The medium intensity peak due to symmetric and asymmetric stretching of C-H bonds present in lengthy alkyl chain is observed between 3000 and 2800 cm^{-1} for both functionalized and un-functionalized CNTs. The peak around ~ 1625 cm^{-1} can be attributed to the conjugation of C=O (carbonyl group) with C=C (vibrational mode of CNT skeletal). The medium intensity peak around ~ 1460 cm^{-1} can be attributed to the bending of the –OH bond in the carboxyl group.

The Fenton reaction introduced primarily hydroxyl groups on the graphite nano-flakes. The presence of –OH group attached to graphite nano-flakes was confirmed using FTIR spectroscopy. The strong and broad peak present for

Fig. 4 The FTIR spectra of **a** acid-functionalized MWCNT, **b** un-functionalized MWCNT, **c** graphite flakes, **d** hydroxylated graphene nanoflakes and **e** hybrid 3D nanomaterials
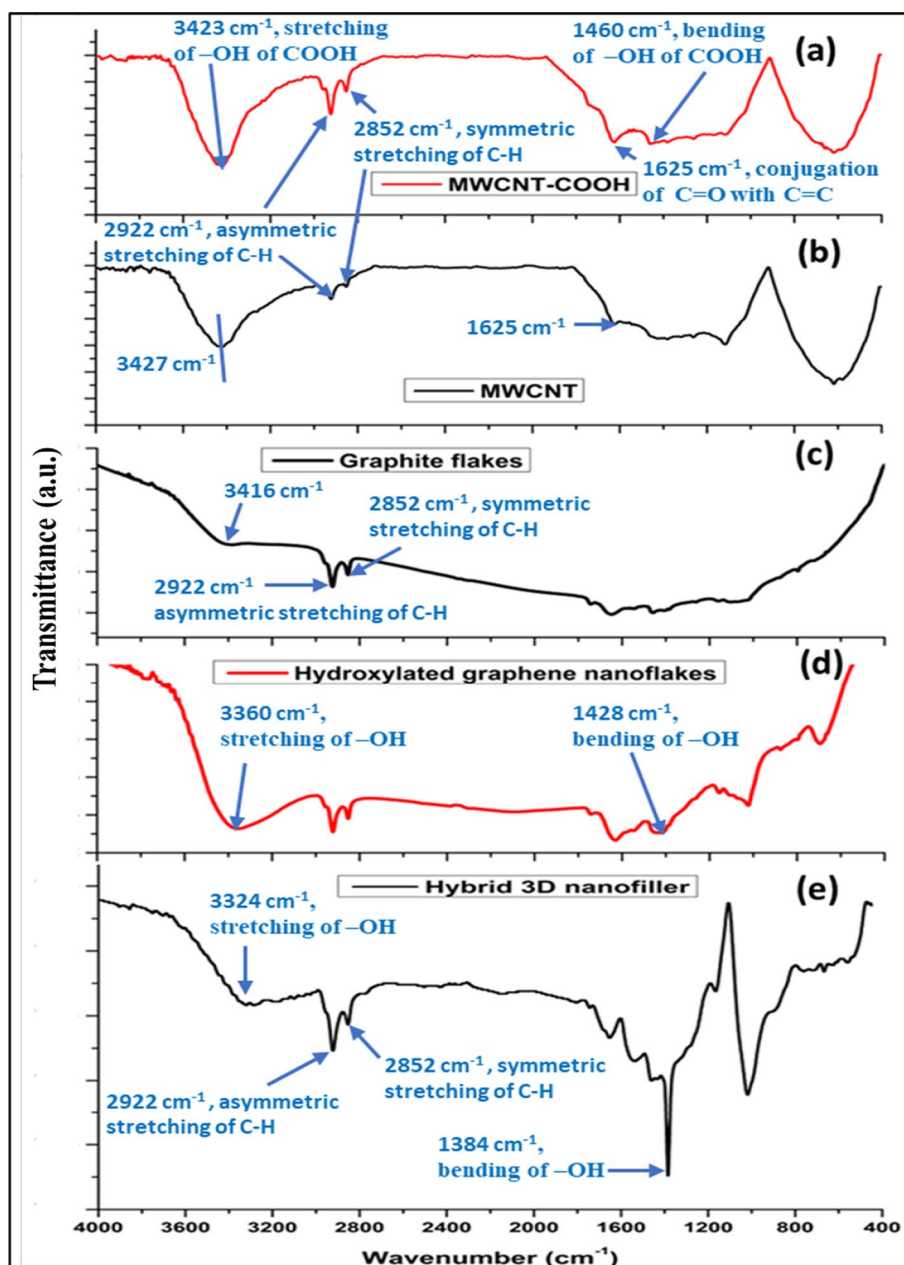
hydroxylated graphite nano-flakes (or edge-functionalized/oxidized FLG flakes) around ~ 3400 cm^{-1} is due to the stretching of the hydroxyl group, as observed in Fig. 4c, d.

The hybrid 3D nanofiller has both hydroxylated graphene nanoflakes and acid-functionalized CNTs. The functional group of acid-functionalized CNTs (–COOH) and that of hydroxylated graphite nano-flakes (–OH) have formed weak bonds, which cause a slight shift in the peak attributed to the stretching of the –OH bond at around ~ 3300 cm^{-1}, as shown in Fig. 4e. This shift in the peak was observed due to the presence of hydrogen-bonded hydroxyl and carboxyl groups that weakens the –OH bond and hydrolowers the absorption frequency. The peak around ~ 1400 cm^{-1} is due to the bending of the –OH bond in the carboxyl group.

The hydrogen bonding in hybrid 3D nanomaterial due to the presence of the hydroxyl group of FLG and the carboxyl group of acid-functionalized MWCNT made the 3D nanomaterials chemically more stable.

3.2 X-Ray photoelectron spectroscopy (XPS)

XPS is a surface analytical technique, and it gives information regarding chemical bonding on the surface of the nanofillers. The acid-functionalized MWCNTs and the edge-functionalized/oxidized FLG flakes were synthesized in the laboratory. This analysis can determine the nature of oxygen-containing functional groups attached on the surface, and also if there are any structural defects present on the nanofillers surface.

For the MWCNTs, the peak at 284 eV was attributed to the C=C bond or sp^2 hybridized carbon, and the peak at 285.5 eV was attributed to the C–C bond or sp^3 hybridized carbon, as shown in Fig. 5b. The XPS spectra of the acid-functionalized MWCNTs show peaks at 284 eV (C=C bond) and 285.5 eV (C–C bond), similar to MWCNTs. The slight reduction in the intensity of the sp3 hybridized carbon peak shows a reduction in amorphous carbons in pristine MWCNTs by acid functionalization. The presence of carboxyl group (–COOH) attached to the surface of the acid-functionalized MWCNTs was confirmed by the peak at 286.5 eV attributed to C–O and a peak at 287.5 eV attributed to C=O, as observed in Fig. 5a.

The XPS spectra of the graphite flakes and the edge-functionalized/oxidized FLG flakes were compared. The graphite flakes XPS spectra, as shown in Fig. 5d, show a peak at 284.3 eV that can be attributed to the C=C bond, and a peak at 285.5 eV that can be attributed to the C–C bond. After the edge functionalization of the FLG flakes with hydroxyl groups, the XPS spectra show the usual peaks at 284.5 eV (C=C bond), and the peak at 285.3 eV (C–C bond), as shown in Fig. 5c. The intensity of the sp^3 hybridized carbon (C–C) peak, associated with defects on the surface, has increased very slightly in the case of FLG flakes. The presence of hydroxyl group (–OH) in FLG flakes was confirmed by the presence of a peak at 289 eV that was attributed to the C–O bond.

3.3 Electron microscopy

Transmission Electron Microscopy (TEM) and Scanning Electron Microscopy (SEM) are used to study the morphology of the nanomaterials and the changes in morphology on the functionalization of the nanomaterials.

SEM and TEM were utilized to identify the alteration in the morphology of MWCNTs before and after functionalization. Before the functionalization, the MWCNTs were agglomerated and no specific nanotubes could be observed, as seen in Fig. 6a. After the functionalization of the MWCNTs, they appear to have de-agglomerated to a certain degree as observed in the SEM image, shown in Fig. 7b. The tube-like structures of the MWCNTs can be observed in the TEM image of acid-functionalized MWCNTs, as shown in Fig. 7a.

The functional groups help to disperse and de-agglomerate the acid-functionalized MWCNTs, which can be concluded by comparing the SEM images of MWCNTs before functionalization, as shown in Fig. 6a, and after functionalization, as shown in Fig. 7b.

The morphology of the graphite flakes and edge-functionalized FLG flakes were observed using electron microscopy. The size of the graphite flakes was very large as observed in the SEM image at 5 µm magnification, as shown in Fig. 6b. A graphite flake is made up of numerous graphene layers. The edge functionalization causes the exfoliation of the graphite flakes, thus reducing the size and the number of graphene layers in the graphite. The FLG nano-flakes have been prepared with reduced size and thickness, which can be observed from the SEM image, as shown in Fig. 7d. The TEM image of the FLG flake evidently shows the presence of only a few graphene sheets, as shown in Fig. 7c.

The hybrid 3D nanomaterial is formed by mixing together FLG flakes and functionalized MWCNTs. The carboxyl groups (–COOH) attached to the acid-functionalized MWCNTs form hydrogen bonds.

with the hydroxyl groups (–OH) attached to the FLG flakes. Thus, immobilizing the MWCNTs between different FLG flakes and forming a 3D structure can be observed from the TEM image of 3D nanomaterials at 100 nm magnification, as

Fig. 5 The XPS spectra of **a** acid-functionalized MWCNTs, **b** MWCNTs, **c** hydroxylated graphene nanoflakes (FLG), and **d** graphite flakes
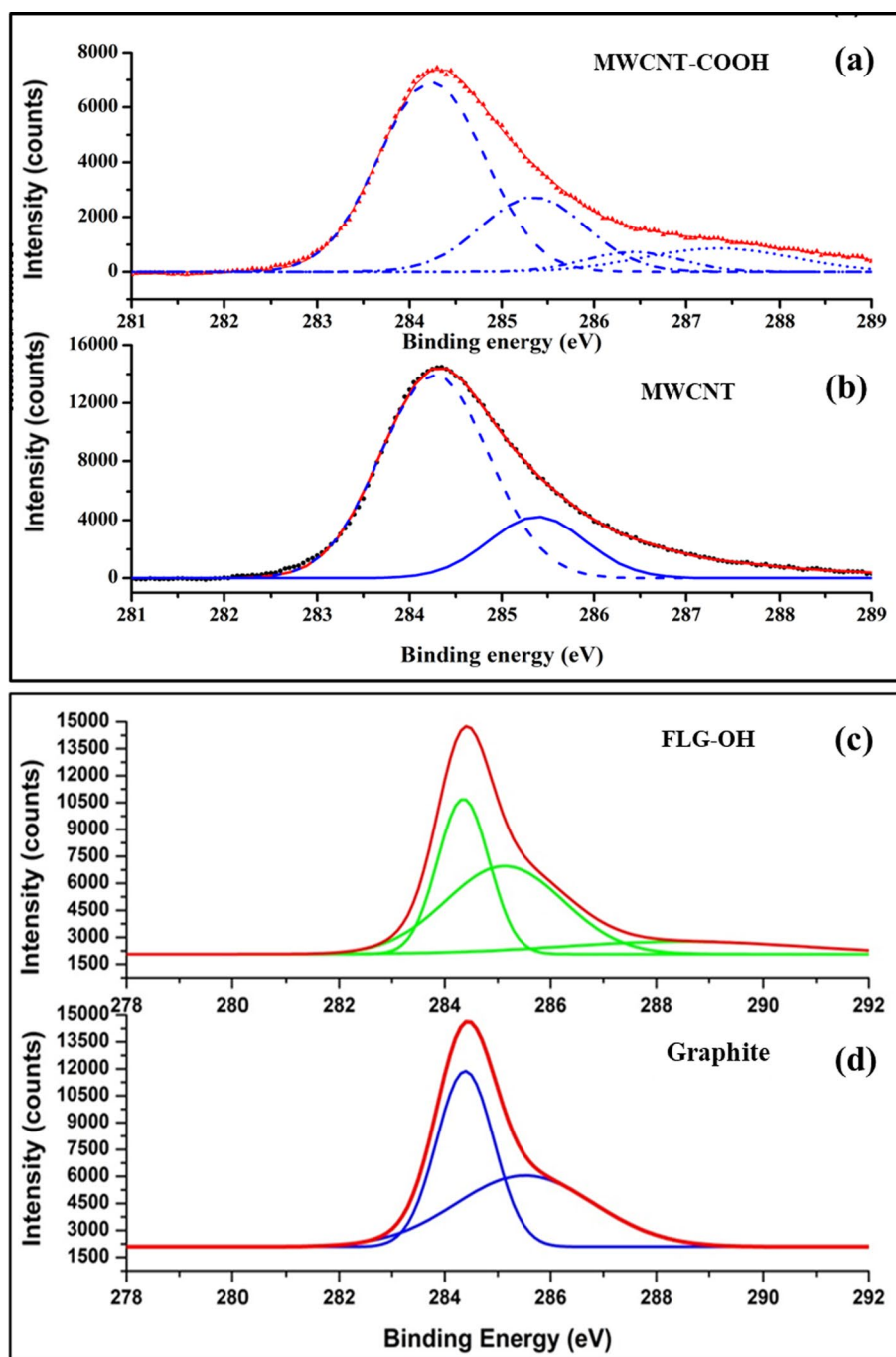

shown in Fig. 7e. It can be observed from the SEM image that the MWCNTs that have been restrained on the FLG flakes, are due to the formation of weak bonds, as shown in Fig. 7f.

In hybrid 3D nanomaterials, it was observed that the acid-functionalized MWCNTs penetrated into the hydroxylated FLGs. The immobilized acid-functionalized MWCNTs into the hydroxylated FLGs of hybrid 3D nanomaterials which is the key factor for the high exfoliation and dispersion of FLGs.

3.4 Thermogravimetric analysis (TGA)

The thermal stability of the nanomaterials was observed using the TGA analysis. This is because the different carbon structures demonstrate different behaviour during oxidation which depends each time on the reactive sites that are available.
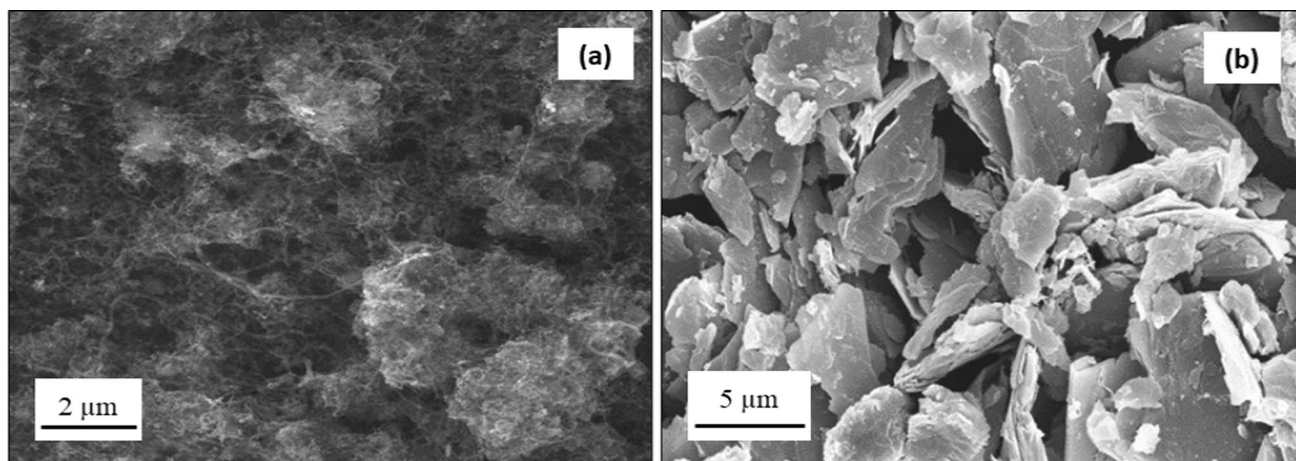
Fig. 6 The SEM images of **a** un-functionalized MWCNTs at 2 µm magnification; and **b** graphite flakes at 5 µm magnification

The treatment of the as-received MWCNTs using acids mixture (H_2SO_4 and HNO_3), causes the end of the MWCNTs to open up, and the functional groups, like carboxyl groups (–COOH), gets attached at those ends. The functional groups are also attached at the CNTs defects sites. The TGA thermograms of MWCNTs and functionalized MWCNTs are compared in Fig. 8a. The MWCNTs were observed to be thermally stable up to a range of ~ 350 °C. Beyond this temperature, the MWCNTs begins decomposing and between the temperature range of 375–525 °C, the MWCNTs loses ~ 90% of its mass.

This was attributed to the presence of amorphous or disordered carbons, which have a tendency to get oxidized at higher temperature, due to the existence of either large quantities of active sites or due to the lower energy required for their oxidation. The functionalized MWCNTs were observed to be stable up to ~ 275 °C. There was a sharp loss of 80% mass in a range of 350–450 °C which was attributed to the oxidation of carbon framework. The functionalized MWCNTs have carboxyl groups attached to it which decomposes at lower temperature. This causes the decomposition temperature of functionalized MWCNTs to shift to a lower temperature as compared to pristine MWCNTs.

The comparison of the thermal stability of the hydroxylated FLG flakes and graphite is shown in Fig. 8b. Hydroxylated FLG flakes lose ~ 9% of mass between 30 and 150 °C, which can be attributed to the evaporation of absorbed moisture. Graphite is more thermally stable upto 600 °C, whereas the hydroxylated FLG flakes lose ~ 55% of its mass and oxidized faster in the same range, as observed in Fig. 8b. This can be attributed to the decomposition of the hydroxyl groups attached to the edge-functionalized/oxidized FLG flakes. Towards the end of the TGA analysis at ~ 800 °C, the FLG flakes had ~ 40% residue due to the presence of iron (Fe) particles that came from the Fenton's reagent.

The hybrid 3D nanomaterial thermally decomposes in three stages, as seen in Fig. 9. In the temperature range of ~ 30–75 °C, the 3D nanomaterial suffers a ~ 5% loss in mass which can attributed to the evaporation of any absorbed moisture. It was observed to be thermally stable in the range of 75–175 °C. It loses ~ 7.5% of its mass in the temperature range of ~ 175–250 °C which can be attributed to the oxidation of ooxygen-containing functional groups at higher temperatures. The 3D nanomaterials did not lose any mass in the range of ~ 250–550 °C, due to the stable structure. There was a loss of ~ 70% mass in the range of ~ 550–800 °C, due to the oxidation of stable graphitic structure at a much higher temperature. Towards the end of the TGA analysis at ~ 800 °C, the 3D nanomaterial had ~ 8% residue. The lower iron residue in 3D nanomaterials can be explained in terms of the process adapted to prepare the 3D structures where both 1D and 2D nanomaterials were sonicated in organic solvent to prepare hierarchical morphology.

3.5 X-Ray diffraction (XRD)

The comparison of the X-ray diffraction (XRD) spectra of the MWCNT and the acid-functionalized MWCNT is shown in Fig. 10a. The typical peaks at (002) and (100) of MWCNT are obtained at 2θ of 26° and 43°, respectively, as shown in Fig. 10a. The graphite peak at (002) is attributed to the graphitic structure of CNTs.

The comparison of XRD spectra of graphite and edge functionalized FLG flakes has been shown in Fig. 10b. The sharp diffraction peak (002) at 2θ = 26.5° is due to the graphitic structure, shown by both graphite flakes and FLG flakes. The intensity of (002) peak of the graphite flakes is higher than that of FLG. This shows that compared to the graphite flakes, the graphitic structure of FLG flakes has been disrupted.
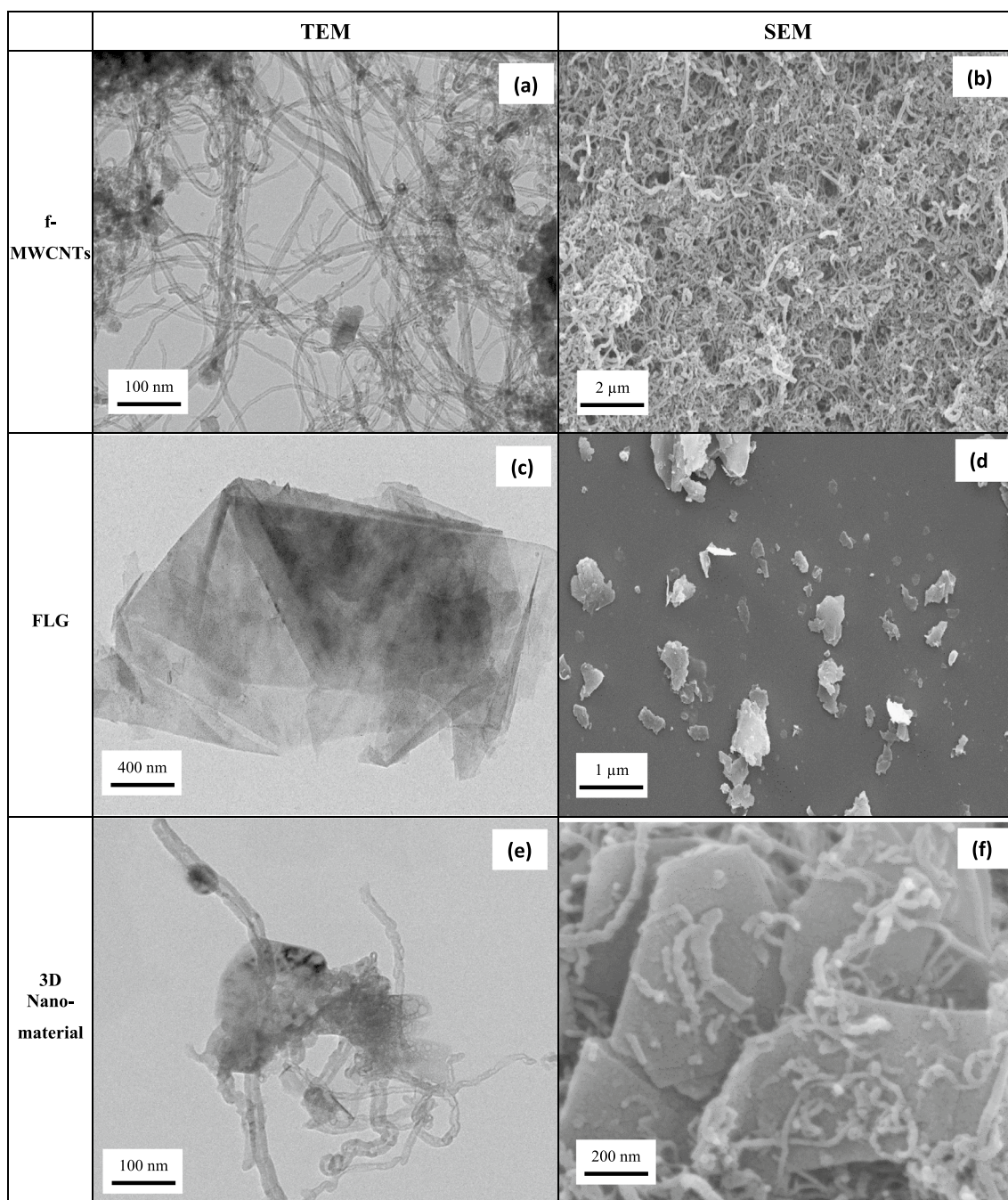
Fig. 7 The Electron Microscopy images of the synthesized nanomaterials. **a** TEM image of acid-functionalized MWCNTs (f-MWCNTs) at 100 nm magnification; **b** SEM image of acid-functionalized MWCNTs (f-MWCNTs) at 2 μm magnification; **c** TEM image of edge-functionalized/oxidized FLG flakes at 400 nm magnification; **d** SEM image of edge-functionalized/oxidized FLG flakes at 1 μm magnification; **e** TEM image of hybrid 3D nanomaterials at 100 nm magnification; and **f** SEM images of hybrid 3D nanomaterials at 200 nm magnification

The XRD spectra of the 3D nanomaterials have been compared with those of acid-functionalized MWCNTs and edge-functionalized FLG flakes, as shown in Fig. 11. The peak of the 3D nanomaterial is obtained at $2\theta = 26.5^{\circ}$ which is attributed to the graphitic structure, as seen in Fig. 11. In comparison to functionalized MWCNTs and the 3D nanomaterial, the peak of FLG flakes has the highest intensity. This can be attributed to the presence of more unharmed graphitic surfaces in FLG flakes when compared to 3D and functionalized MWCNTs.

The peal observed at $2\theta = 26.5^{\circ}$ for the hybrid 3D nanomaterial is asymetrical, which could be partially assigned to the functionalized MWCNTs and the edge-functionalized FLG, respectively .

Fig. 8 The comparative TGA thermograms of **a** MWCNT and acid functionalized MWCNT, and **b** graphite and hydroxylated FLG flakes
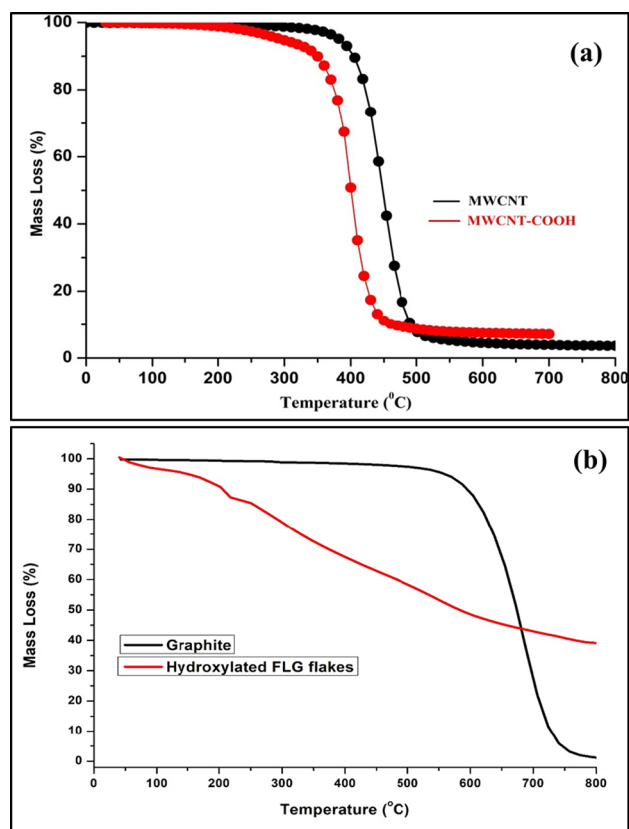
**Fig. 9** The TGA thermogram of 3D hybrid nanomaterial
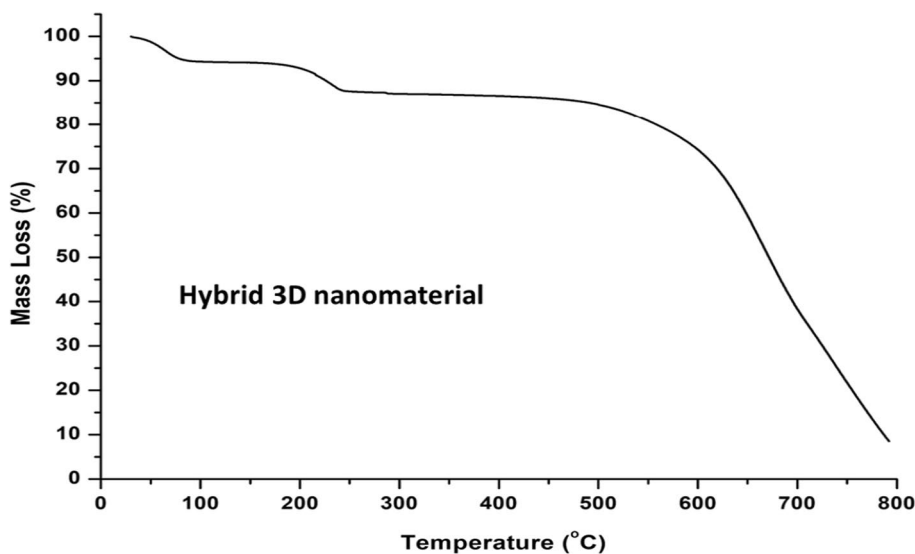

3.6 Raman spectroscopy

Raman spectroscopy is a technique that was utilized for the characterization of carbon nanoparticles. The Raman spectra of the MWCNTs and the acid-functionalized MWCNTs are compared, as shown in Fig. 12a. The characteristic bands shown by both un-functionalized and functionalized MWCNTs are D-band and G-band. The D-band is a disorder-induced feature caused to double resonance Raman scattering process from a non-zero-center phonon mode [47, 48].

The D-band is attributed to the presence of disordered or amorphous carbons in the MWCNTs. The G-band is obtained due to in-plane tangential stretching of the C–C bonds in graphene sheets. In the case of un-functionalized

Fig. 10 The XRD of **a** MWCNT and acid functionalized MWCNT, and **b** graphite and edge functionalized FLG flakes
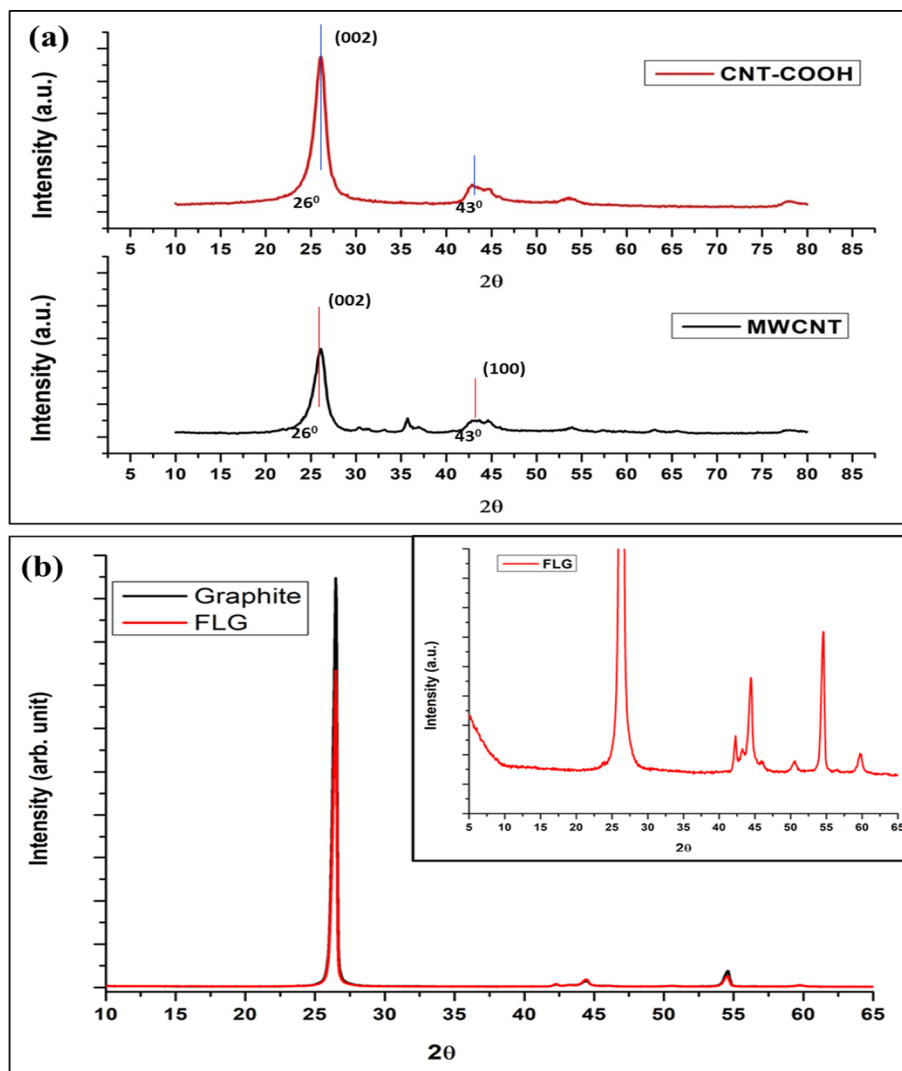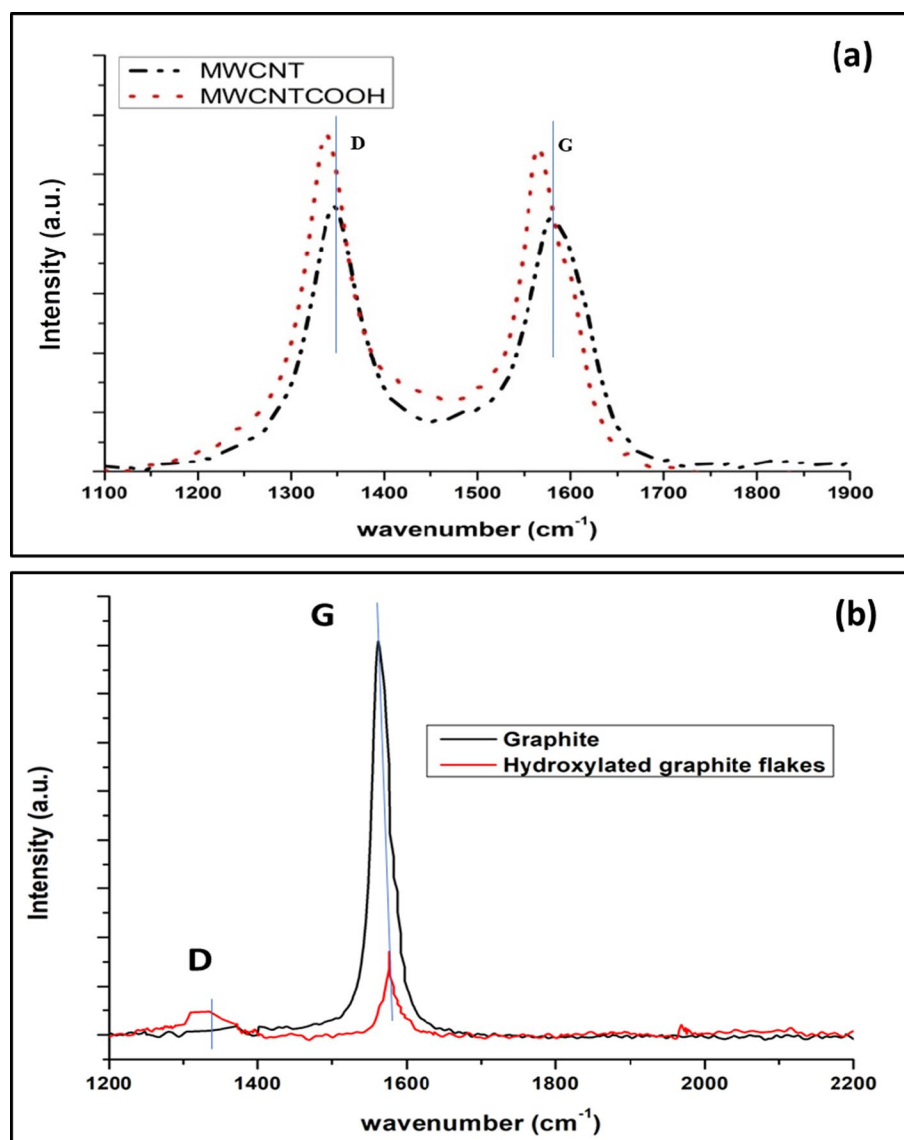

Fig. 11 The comparison of XRD spectra of acid-functionalized MWCNTs, edge-functionalized FLG flakes and hybrid 3D nanomaterials
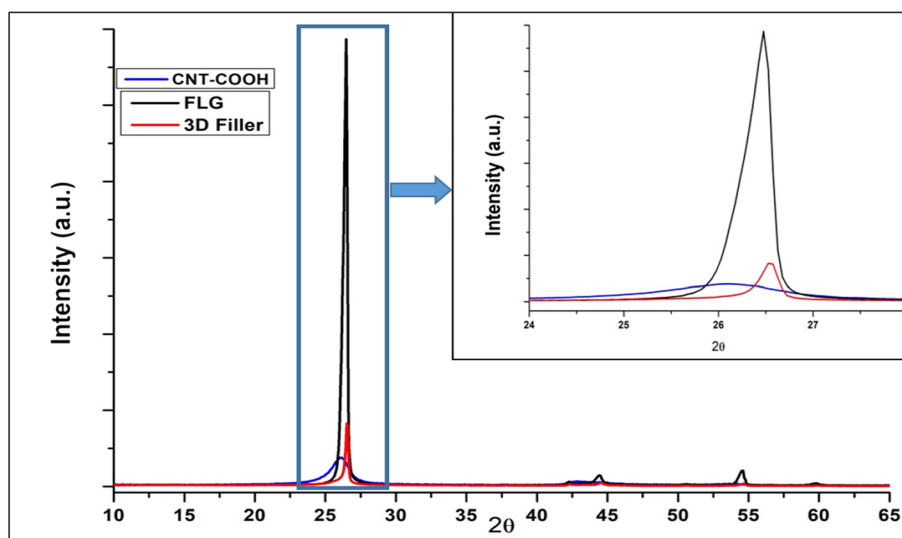
Fig. 12 Raman spectra of **a** MWCNTs and acid-functionalized MWCNTs, and **b** graphite flakes and hydroxylated graphite flakes have been presented in the frequency range of 1100–1900 cm^{-1}

MWCNTs, the D-band is obtained at ~ 1350 cm^{-1} and the G-band is obtained at ~ 1580 cm^{-1}. After the acid functionalization of MWCNTs, their Raman spectra show an increase in the intensity of the D-band as well as reduction in the intensity of the G-band. The acid-functionalization is a harsh oxidative treatment that leads to more disordered carbons in the MWCNTs after functionalization with acids. The G-band is sensitive to minor strains and the shift in this band in the case of acid-functionalized MWCNTs can be attributed to the addition of the functional groups on MWCNTs. I_D/I_G ratio for MWCNT is 1.045 and MWCNTs-COOH is 1.074.

In the case of graphite flakes, the D-band is obtained at ~ 1375 cm^{-1} and the G-band is obtained at ~ 1570 cm^{-1}, as shown in Fig. 12b. The edge-functionalized FLG flakes were prepared using graphite flakes and Fenton's reagent. The Raman spectra of FLG flakes show that the intensity of the D-band has increased and the G-band has decreased. In the case of FLG flakes, the increase in the intensity of the D-band is attributed to defects generated due to sp^3 hybridization of carbon atoms. The slight shift in the G-band of FLG flakes compared to graphite can be attributed to the reduction in the number of graphene layers. I_D/I_G ratio for graphite flakes is 0.04 and the same for FLG flakes is 0.21.

4 Conclusion

The synthesis of the acid functionalized MWCNTs prepared via strong oxidative treatment of pristine MWCNTs, using the acid mixture (HNO_3/H_2SO_4). The FTIR spectra confirmed the presence of carboxyl group (–COOH) in acid functionalized MWCNTs by peak formed due to stretching of the –OH bond around ~ 3400 cm^{-1}. The same was confirmed using the XPS analysis whose spectra shows the presence of the peak at 286.5 eV attributed to C–O and a peak at 287.5 eV attributed to C = O in functionalized MWCNTs. The SEM and TEM images of pristine MWCNTs and acid-functionalized MWCNTs were compared and it was observed that the functionalization causes the MWCNTs to de-agglomerate. Thus, it is shown that functionalization assists in better dispersion due to the presence of functional groups that prevents the agglomeration. The XRD spectra comparison of the MWCNTs before and after function-alization shows that the intensity of the (002) peak increases in the case of acid functionalized MWCNTs due to the reduction of amorphous carbon in pristine MWCNTs. The TGA of the MWCNTs before and after functionalization shows that the oxidation of the carboxyl functional group attached to functionalized MWCNT causes an early onset of decomposition compared to that of pristine MWCNTs.

The edge-functionalized FLG flakes were prepared by reacting graphite with the Fenton's reagent which causes the hydroxyl groups to be attached to the edges of the as-synthesized FLG flakes of the graphite. The FTIR spectra of graphite and the edge functionalized/oxidized FLG flakes were compared. The presence of the hydroxyl group, on the edge func-tionalized/oxidized FLG flakes, as a strong and broad peak around ~ 3400 cm^{-1} was confirmed using the FTIR analysis. The XPS spectra of the FLG show the presence of hydroxyl group (–OH) by the presence of peak at 289 eV that was attributed to C–O bond. The XRD spectra of the graphite and the edge functionalized/oxidized FLG flakes was compared and it was observed that the intensity of the (002) peak was reduced in the case of edge functionalized/oxidized FLG flakes. Their SEM and TEM images were compared and their surface morphology was observed. It was observed that along with reduced size and thickness, the edge-functionalized/oxidized FLG flakes was made up of few layers of graphene, compared to graphite. Their Raman spectra show that the number of layers has been reduced in the case of FLG flakes. Their thermal stability was observed using the TGA, and it was observed that the decomposition temperature of the edge-functionalized/oxidized FLG flakes shifted to a lower temperature compared to graphite due to the presence of the functional group. The graphite was observed to be stable up to 600 °C.

The hybrid 3D nanomaterial was synthesized using the functionalized MWCNTs and the edge-functionalized/oxi-dized FLG flakes. The FTIR spectra of 3D nanomaterial show the presence of hydroxyl peak at ~ 3300 cm^{-1}. The shift of the peak of –OH bond was attributed to the weak bonds between the hydroxyl and carboxyl groups. The SEM and TEM images of the 3D nanomaterial confirm that it has formed by immobilizing the functionalized MWCNTs into the edge-functionalized/oxidized FLG flakes. The TGA of the 3D nanomaterial shows that it is almost stable upto ~ 575 °C after which it loses ~ 70% mass in the range of 575–800 °C due to the oxidation of stable graphitic structure at a much higher temperature. The comparison of TGA thermogram confirms that the 3D nanomaterial is more thermally stable than functionalized MWCNTs and FLG flakes. The XRD spectrum of the 3D nanomaterial was obtained at 26.5^0, which is similar to that of functionalized MWCNTs and edge-functionalized/oxidized FLG flakes.

The various characterization techniques viz. SEM, TEM and XRD showed the porous and exfoliated hybrid 3D nano-material prepared by immobilizing acid-functionalized MWCNTs into the hydroxylated FLGs. The FT-IR spectra indicate a stable morphology of 3D hierarchical structure made of functional 1D and 2D nanomaterials by hydrogen bonding.

Author contributions Conceptualization: Subhash Mandal, Debmalya Roy and Mangala Joshi; methodology: Subhash Mandal, Debmalya Roy and Mangala Joshi; formal analysis and investigation: Subhash Mandal, Ratna Singh, Debmalya Roy, Kingsuk Mukhopadhyay, Mayank Dwivedi and Mangala Joshi; writing—original draft preparation: Subhash Mandal; writing—review and editing: Ratna Singh, Debmalya Roy, Kingsuk Mukhopadhyay, Mayank Dwivedi and Mangala Joshi; funding acquisition: Nil; resources: Debmalya Roy, Kingsuk Mukhopadhyay, Mayank Dwivedi and Mangala Joshi; supervision & design of experiments: Debmalya Roy and Mangala Joshi.

Data availability The data used and analysed during this study are available from the corresponding author on reasonable request. The authors declare that all other data supporting the findings of this study are available within the paper.

Discover

Declarations

Competing interests There is no competing interests.

Open Access This article is licensed under a Creative Commons Attribution 4.0 International License, which permits use, sharing, adaptation, distribution and reproduction in any medium or format, as long as you give appropriate credit to the original author(s) and the source, provide a link to the Creative Commons licence, and indicate if changes were made. The images or other third party material in this article are included in the article's Creative Commons licence, unless indicated otherwise in a credit line to the material. If material is not included in the article's Creative Commons licence and your intended use is not permitted by statutory regulation or exceeds the permitted use, you will need to obtain permission directly from the copyright holder. To view a copy of this licence, visit http://creativecommons.org/licenses/by/4.0/.

References

1. Iijima S. Helical microtubules of graphitic carbon. Nature. 1991;354:56–8.
2. Dresselhaus MS, Dresselhaus G, Saito R. Physics of carbon nanotubes. Carbon. 1995;33:883–91.
3. Datsyuk V, Kalyva M, Papagelis K, Parthenios J, Tasis D, Siokou A, Kallitsis I, Galiotis C. Chemical oxidation of multiwalled carbon nanotubes. Carbon. 2008;46:833–40.
4. Zhang N, Xie J, Varadan VK. Functionalization of carbon nanotubes by potassium permanganate assisted with phase transfer catalyst. Smart Mater Struct. 2002;11:962–5.
5. Siegrist RL, West OR, Crimi ML, Lowe KS. Principles and practices of in situ chemical oxidation using permanganate. Columbus: Battelle Press; 2001.
6. Fukushima H, Drzal LT.A carbon nanotube alternative: Graphite nanoplatelets as reinforcements for polymers. Ann Tech Conf – Soc Plast Eng. 2003; 2230–4.
7. Kotov NA. Materials science: carbon sheet solutions. Nature. 2006;442:254–5.
8. Hernandez Y, Nicolosi V, Lotya M, Blighe FM, Sun Z, De S, McGovern IT, Holland B, Byrne M, Gun'Ko YK, et al. High-yield production of graphene by liquid-phase exfoliation of graphite. Nat Nanotechnol. 2008;3:563–8.
9. Skaltsas T, Ke X, Bittencourt C, Tagmatarchis N. Ultrasonication induces oxygenated species and defects onto exfoliated graphene. J Phys Chem C. 2013. https://doi.org/10.1021/jp4057048.
10. Novoselov KS, Falko VI, Colombo L, Gellert PR, Schwab MG, Kim K. A roadmap for graphene. Nature. 2012;490:192–200.
11. Bai H, Li C, Shi G. Functional composite materials based on chemically converted graphene. Adv Mater. 2011;23:1089–115.
12. Hummers WS, Offeman R. Preparation of graphitic oxide. J Am Chem Soc. 1958;80:1339. https://doi.org/10.1021/ja01539a017.
13. Brodie BC. On the atomic weight of graphite. Philos Trans R Soc Lond. 1859;14:249–59.
14. Staudenmaier L. Verfahren zur darstellung der graphitsaure. Ber Dtsch Chem Ges. 1898;31:1481–7.
15. Chen J, Yao B, Li C, Shi G. An improved Hummers method for eco-friendly synthesis of graphene oxide. Carbon. 2013;64:225–9. https://doi.org/10.1016/j.carbon.2013.07.055.
16. Schniepp HC, Li J-L, McAllister MJ, Sai H, Herrera-Alonso M, Adamson DH, et al. Functionalized single graphene sheets derived from splitting graphite oxide. J Phys Chem B. 2006;110:8535–9.
17. Bourlinos AB, Gournis D, Petridis D, Szabo T, Szeri A, Dekany I. Graphite oxide: chemical reduction to graphite and surface modification with primary aliphatic amines and amino acids. Langmuir. 2003;19:6050–5.
18. Kotov NA, Dekany I, Fendler JH. Ultrathin graphite oxidepolyelectrolyte composites prepared by self-assembly. Transition between conductive and non-conductive states. Adv Mater. 1996;8:637–41.
19. Xiao P, Xiao M, Liu P, Gong K. Direct synthesis of a polyaniline-intercalated graphite oxide nanocomposite. Carbon. 2000;38:626–8.
20. Becerril HA, Mao J, Liu Z, Stoltenberg RM, Bao Z, Chen Y. Evaluation of solution-processed reduced graphene oxide films as transparent conductors. ACS Nano. 2008;2:463.
21. Eda G, Fanchini G, Chhowalla M. Large-area ultrathin films of reduced graphene oxide as a transparent and flexible electronic material. Nat Nanotechnol. 2008;3:270.
22. Wang X, Zhi L, Mullen K. Transparent, conductive graphene electrodes for dye-sensitized solar cells. Nano Lett. 2008;8:323.
23. Stankovich S, Dikin DA, Piner RD, Kohlhaas KA, Kleinhammes A, Jia Y, Wu Y, Nguyen SBT, Ruoff RS. Synthesis of graphene-based nanosheets via chemical reduction of exfoliated graphite oxide. Carbon. 2007;45:1558–65. https://doi.org/10.1016/j.carbon.2007.02.034.
24. Shin H-J, Kim KK, Benayad A, Yoon S-M, Park HK, Jung I-S, Jin MH, Jeong H-K, Kim JM, Choi J-Y, Lee YH. Efficient reduction of graphite oxide by sodium borohydride and its effect on electrical conductance. Adv Funct Mater. 2009. https://doi.org/10.1002/adfm.200900167.
25. Shen J, Hu Y, Shi M, Lu X, Qin C, Li C, Ye M. Fast and facile preparation of graphene oxide and reduced graphene oxide nanoplatelets. Chem Mater. 2009;21:3514–20. https://doi.org/10.1021/cm901247t.
26. Si Y, Samulski ET. Synthesis of water soluble graphene. Nano Lett. 2008;8:1679–82.
27. Loeffler HJ, Ponting JD. Ascorbic acid. Ind Eng Chem Anal Ed. 1942;14:846–9.
28. Ambrosi M, Fratini E, Alfredsson V, Ninham BW, Giorgi R, Nostro PL, Baglioni P. Nanotubes from a Vitamin C-Based Bolaamphiphile. J Am Chem Soc. 2006;128:7209–14.
29. Wang Y, Camargo PHC, Skrabalak SE, Gu H, Xia Y. A facile, water-based synthesis of highly branched nanostructures of silver. Langmuir. 2008;24:12042–6.
30. Zhang J, Yang H, Shen G, Cheng P, Zhang J, Guo S. Reduction of graphene oxide via L-ascorbic acid. Chem Commun. 2010;46:1112–4. https://doi.org/10.1039/b917705a.
31. Ioni Y, Sapkov I, Kirsanova M, Dimiev AM. Flame modified graphene oxide: Structure and sorption properties. Carbon. 2023;1(212):118122.
32. Li D, Muller MB, Gilje S, Kaner RB, Wallace GG. Processable aqueous dispersions of graphene nanosheets. Nat Nanotechnol. 2008;3:101–5.

33. Park S, Ruoff RS. Chemical methods for the production of graphenes. Nat Nanotechnol. 2009;4:217–24.

34. Fenton HJH. Oxidation of tartaric acid in the presence of iron. J Chem Soc. 1894;65:899–910.

35. Zhou X, Zhang Y, Wang C, Wu X, Yang Y, Zheng B, Wu H, Guo S, Zhang J. Photo-fenton reaction of graphene oxide: a new strategy to prepare graphene quantum dots for DNA cleavage. ACS Nano. 2012. https://doi.org/10.1021/nn301629v.

36. Bauer R, Fallmann H. The photo-fenton oxidation -a cheap and efficient wastewater treatment method. Res Chem Intermed. 1997;23:341–54.

37. Liu C, Li J, Qi J, Wang J, Luo R, Shen J, Sun X, Han W, Wang L. Yolk–Shell Fe0@SiO2 nanoparticles as nanoreactors for fenton-like catalytic reaction. ACS Appl Mater Interfaces. 2014;6:13167–73.

38. Shin S, Yoon H, Jang J. Polymer-encapsulated iron oxide nanoparticles as highly efficient Fenton catalysts. Catal Commun. 2008;10:178–82.

39. Jun LY, Mubarak NM, Yon LS, Bing CH, Khalid M, Abdullah EC. Comparative study of acid functionalization of carbon nanotube via ultrasonic and reflux mechanism. J Environ Chem Eng. 2018;6(5):5889–96.

40. Pistone A, Ferlazzo A, Lanza M, Milone C, Iannazzo D, Piperno A, Piperopoulos E, Galvagno S. Morphological modification of MWCNT functionalized with HNO3/H2SO4 mixtures. J Nanosci Nanotechnol. 2012;12(6):5054–60.

41. Deng H, Huang J, Qin C, Xu T, Ni H, Ye P. Preparation of high-performance nanocomposite membranes with hydroxylated graphene and graphene oxide. J Water Process Eng. 2021;40:101945.

42. Sun J, Deng Y, Li J, Wang G, He P, Tian S, Bu X, Di Z, Yang S, Ding G, Xie X. A new graphene derivative: hydroxylated graphene with excellent biocompatibility. ACS Appl Mater Interfaces. 2016;8(16):10226–33.

43. Ding JH, Rahman O, Zhao H, Peng W, Dou H, Chen H, Yu H. Ultrahigh electrical and thermal conductive hydroxylated graphene-based flexible carbon film. Nanotechnology. 2017;28:39LT01.

44. Tiwari N, Agarwal N, Roy D, Mukhopadhyay K, Prasad NE. Tailor made conductivities of polymer matrix for thermal management: design and development of topologically controlled hierarchical nanostructures. Ind Eng Chem Res. 2017;56:672–9.

45. Agarwal N, Bhattacharyya R, Tripathi NK, Kanojia S, Roy D, Mukhopadhyay K, Prasad NE. Derivatization and interlaminar debonding of graphite–iron nanoparticle hybrid interfaces using Fenton chemistry. Phys Chem Chem Phys. 2017;19(25):16329–36.

46. Xing Y. Synthesis and electrochemical characterization of uniformly-dispersed high loading Pt nanoparticles on sonochemically-treated carbon nanotubes. J Phys Chem B. 2004;108:19255–9. https://doi.org/10.1021/jp046697i.

47. Thomsen C, Reich C. Double resonant Raman scattering in graphite. Phys Rev Lett. 2000;85:5214–7.

48. Dresselhaus MS, Dresselhaus G, Saito R, Jorio A. Raman spectroscopy of carbon nanotubes. Phys Rep. 2005;409:47–99.